The Astrophysical Journal, 834:107 (15pp), 2017 January 10 doi:10.3847/1538-4357/834/2/107

COMMON ENVELOPE EJECTION FOR A LUMINOUS RED NOVA IN M101

N. Blagorodnova[1,2], R. Kotak[3], J. Polshaw[3], M. M. Kasliwal[1], Y. Cao[1], A. M. Cody[4], G. B. Doran[5], N. Elias-Rosa[6], M. Fraser[2], C. Fremling[7], C. Gonzalez-Fernandez[2], J. Harmanen[8], J. Jencson[1], E. Kankare[3], R.-P. Kudritzki[9], S. R. Kulkarni[1], E. Magnier[9], I. Manulis[10], F. J. Masci[1], S. Mattila[2,8], P. Nugent[11], P. Ochner[6], A. Pastorello[6], T. Reynolds[8,12], K. Smith[3], J. Sollerman[7], F. Taddia[7], G. Terreran[3,6], L. Tomasella[6], M. Turatto[6], P. M. Vreeswijk[10], P. Wozniak[13], and S. Zaggia[6]

[1] Cahill Center for Astrophysics, California Institute of Technology, Pasadena, CA 91125, USA
[2] Institute of Astronomy, University of Cambridge, Madingley Road, Cambridge CB3 0HA, UK
[3] Astrophysics Research Centre, School of Mathematics and Physics, Queen's University Belfast, Belfast BT7 1NN, UK
[4] Spitzer Science Center, California Institute of Technology, 1200 East California Boulevard, Pasadena, CA 91125, USA
[5] Jet Propulsion Laboratory, California Institute of Technology, Pasadena, CA 91125, USA
[6] INAF-Osservatorio Astronomico di Padova, Vicolo dell Osservatorio 5, I-35122 Padova, Italy
[7] Department of Astronomy, The Oskar Klein Center, Stockholm University, AlbaNova, SE-10691 Stockholm, Sweden
[8] Tuorla Observatory, Department of Physics and Astronomy, University of Turku, Väisäläntie 20, FI-21500 Piikkiö, Finland
[9] Institute for Astronomy, University of Hawaii, 2680 Woodlawn Drive, Honolulu, HI 96822, USA
[10] Department of Particle Physics and Astrophysics, Weizmann Institute of Science, Rehovot 7610001, Israel
[11] Lawrence Berkeley National Laboratory, Berkeley, CA 94720, USA
[12] Nordic Optical Telescope, Apartado 474, E-38700 Santa Cruz de La Palma, Spain
[13] Los Alamos National Laboratory, MS-D466, Los Alamos, NM 87545, USA
Received 2016 July 22; revised 2016 October 21; accepted 2016 October 26; published 2017 January 6

ABSTRACT

We present the results of optical, near-infrared, and mid-infrared observations of M101 OT2015-1 (PSN J14021678+5426205), a luminous red transient in the Pinwheel galaxy (M101), spanning a total of 16 years. The light curve showed two distinct peaks with absolute magnitudes $M_r \leqslant -12.4$ and $M_r \simeq -12$, on 2014 November 11 and 2015 February 17, respectively. The spectral energy distributions during the second maximum show a cool outburst temperature of ≈3700 K and low expansion velocities (≈−300 km s^{-1}) for the H I, Ca II, Ba II, and K I lines. From archival data spanning 15–8 years before the outburst, we find a single source consistent with the optically discovered transient, which we attribute to being the progenitor; it has properties consistent with being an F-type yellow supergiant with $L \sim 8.7 \times 10^4\ L_\odot$, $T_{\rm eff} \approx 7000$ K, and an estimated mass of M1 $= 18 \pm 1\ M_\odot$. This star has likely just finished the H-burning phase in the core, started expanding, and is now crossing the Hertzsprung gap. Based on the combination of observed properties, we argue that the progenitor is a binary system, with the more evolved system overfilling the Roche lobe. Comparison with binary evolution models suggests that the outburst was an extremely rare phenomenon, likely associated with the ejection of the common envelope of a massive star. The initial mass of the primary fills the gap between the merger candidates V838 Mon ($5-10\ M_\odot$) and NGC 4490-OT ($30\ M_\odot$).

Key words: binaries: close – novae, cataclysmic variables – stars: individual (M101 OT2015-1, PSN J14021678 +5426205) – stars: massive – stars: winds, outflows

Supporting material: machine-readable tables

1. INTRODUCTION

The discovery of an unusually bright and red nova in M31 (M31 RV) in 1988 September (Rich et al. 1989), triggered the attention of astronomers toward an uncommon type of object. Its peak absolute magnitude, $M_{\rm V} = -9.95$, was brighter than a regular nova ($M_{\rm V} = -6$ to -8), but fainter than a supernova ($M_{\rm V} < -14$ mag). The surprisingly cool temperature, similar to an M0-type supergiant, and high ejected mass, placed the object into a potentially different category from known cataclysmic variables eruptions, triggering the need for further theoretical exploration. Since then, transient surveys and discoveries led by amateurs contributed to further populate this luminosity "gap" between classical novae and supernovae (SNe; Kasliwal et al. 2011). To date, the observational diversity of such intermediate luminosity events on long timescales (>20 days) encompasses three main categories: (1) SN impostors, due to eruptions in massive stars such as luminous blue variables (LBV), (2) intermediate luminosity optical (red) transients (ILOT/ILRT), explained as terminal faint explosions, and (3) luminous red novae (LRNe), which are potential stellar mergers.

Luminous nonterminal outbursts of massive stars may sometimes mimic the observational signature of an SN. Consequently, this class of events was named as "SN impostors." Among these, eruptions of LBVs are known to produce intermediate luminosity transients (Humphreys & Davidson 1994), such as Eta Carinae and P Cygni. These classical examples generally inhabit the upper part of the Hertzsprung–Russell (HR) diagram, having bolometric magnitudes brighter than $M_{\rm Bol} = -9.5$ mag, in the supergiant region. Generally, LBV progenitors exhibit giant eruptions with visual changes >2 mag, but they also show nonperiodic variability consistent with the behavior of known LBVs in the LMC: R127 and S Doradus (Wolf 1989; Walborn et al. 2008, and references therein). As a consequence, the progenitor stars are generally living in a dusty environment, caused by previous episodes of mass ejections. The nonterminal eruptions of SN 2009ip (Fraser et al. 2013; Mauerhan et al. 2013; Pastorello

et al. 2013) and UGC 2773 OT2009-1 (Foley et al. 2011; Smith et al. 2016a) are examples of LBVs in their cool eruptive phase.

ILRT, such as SN 2008S (Prieto et al. 2008; Botticella et al. 2009; Thompson et al. 2009), NGC 300 2009OT-1 (Bond et al. 2009; Smith et al. 2011), and iPTF10fqs (Kasliwal et al. 2011) also inhabit the luminous part of the "gap" transient family (Kasliwal 2011). Such events have been interpreted as faint terminal explosions associated to dusty progenitors (Prieto et al. 2008, 2009; Kochanek 2011). The electron-capture SNe scenario has been suggested as a possible mechanism (Botticella et al. 2009). Late-time observations reveal the complete disappearance of their progenitors, suggesting their outburst to be a terminal activity (Adams et al. 2016). However, NGC 300-OT has also been interpreted as being due to accretion on the secondary by Kashi et al. (2010). A survey of massive stars in M33 revealed that the rate of SN 2008S and the NGC 300-OT-like transient events is of the order of ∼20% of the CCSN rate in star-forming galaxies in the local universe ($D_L \lesssim 10$ Mpc) (Thompson et al. 2009). However, the fraction of massive stars with colors similar to the progenitors of these transients is only $\lesssim 10^{-4}$. Khan et al. (2010) showed that similar stars are as rare as one per galaxy. The direct implication is that the heavy dust environment phase is a very short transition phase for many massive stars during their final 10^4 years.

Violent binary interactions in binary systems (including stellar mergers) were suggested as the plausible scenario to explain the nature of the outbursts of LRNe (Iben & Tutukov 1992; Soker & Tylenda 2003; Tylenda et al. 2011; Ivanova et al. 2013a). Nova Scorpii 2008 (V1309 Sco) currently provides the most compelling evidence for a merger scenario in our own Galaxy, as the exponential period decay of the progenitor system could be witnessed from observations spanning several years before the outburst (Mason et al. 2010; Tylenda et al. 2011, 2013; Nandez et al. 2014). V833 Mon, at 6.1 ± 0.6 kpc (Sparks et al. 2008) is another remarkable example of a low-mass stellar merger candidate (Soker & Tylenda 2003), including a spectacular light echo revealed by observations with the *Hubble Space Telescope* (*HST*) (Bond et al. 2003). Some extragalactic examples of discoveries consistent with the merger scenario[14] are M85-OT2006OT-1, the luminous red nova in M31, reported in Kurtenkov et al. (2015) and Williams et al. (2015), and the massive stellar merger NGC 4490 2011OT-1 (Smith et al. 2016b). Pre-explosion photometry of the progenitor systems has allowed us to estimate the mass and evolutionary stage of several progenitor systems. To date, the literature reports a wide range of cases, from $1.5 \pm 0.5\ M_\odot$ for V1309 Sco to $20-30\ M_\odot$ for NGC 4490 2011OT-1 (Smith et al. 2016b). In agreement with the progenitor mass function, the estimated observed Galactic rate of such events is one every few years (∼3 years) for low-luminosity events ($M_V \geqslant -4$) and one every 10−30 years for intermediate luminosity ($-7 \leqslant M_V \leqslant -10$) (Kochanek et al. 2014). Events on the bright end such as NGC 4490 2011OT and M101-OT are expected to be far less common, at most one per century.

In this work, we will discuss the observations and nature of M101 OT2015-1 (hereafter M101-OT), also designated as PSN J14021678+5426205 and iPTF13afz (Cao et al. 2015), an extragalactic transient in the luminosity gap. The discovery of M101-OT was publicly announced via the IAU Central Bureau for Astronomical Telegrams (CBAT) by Dimitru Ciprian Vintdevara on the night of 2015 February 10 to 11 in the outskirts of NGC 5457 (M101).[15] Shortly after, it was confirmed by Stu Parker as an optical transient with an unfiltered magnitude of 16.7. The source also had an independent discovery within the intermediate Palomar Transient Factory (iPTF) survey back in 2013, when the progenitor was identified as a slow rising source (Cao et al. 2015). This paper is organized as follows: in Section 2, we report both pre- and post-discovery optical, near-infrared (NIR) and mid-infrared (MIR) photometry and spectroscopy of M101-OT. In Section 3, we examine the spectroscopic measurements and the characteristics of the progenitor. We discuss possible similarities with other objects and the nature of M101-OT in Section 4. Finally, we present a summary and our conclusions in Section 5.

2. OBSERVATIONS

M101-OT is located ($\alpha_{J2000} = 14^h02^m16^s.78$ $\delta_{J2000} = +54^h26^m20^s.5$) in the outer reaches of a spiral arm of M101, at 3′.41 N and 8′.12 W of the measured position of the galaxy nucleus. The surrounding region shows signs of a young stellar population, displaying bright unresolved emission in the *Galaxy Evolution Explorer* (*GALEX*) survey at 135–280 nm.

We adopt the Cepheid distance to M101 of $D_L = 6.4 \pm 0.2$ Mpc, corresponding to a distance modulus of $\mu = 29.04 \pm 0.05$ (random) ± 0.18 (systematic) mag (Shappee & Stanek 2011). The estimated Galactic reddening at the position of the transient is $E(B-V) = 0.008 \pm 0.001$ mag (from NED[16] adopting Schlafly & Finkbeiner 2011), with $R_V = 3.1$, which corresponds to a mean visual extinction of $A_V = 0.024$ mag. The magnitudes reported in the text and figures of this paper have been corrected for Galactic reddening, but the Tables in the Appendix list the observed magnitudes, i.e., not corrected for extinction. The extinction within the host galaxy is not included. Local extinction to the progenitor is unlikely, as archival NIR photometry of M101-OT agrees well with the Rayleigh–Jeans tail of a single blackbody emission derived from optical measurements. Therefore, we argue that there is no evidence of a strong warm dust-emission component in the environment around the progenitor star.

2.1. Photometry

The location of M101-OT has been serendipitously imaged by numerous telescopes and instruments over the last 15 years (from 2000 to 2015). For example, in 2011, this galaxy received special attention, as it hosted one of the youngest SN Ia discovered to date: SN 2011fe (Nugent et al. 2011). In an attempt to piece together the past evolution on M101-OT, we retrieved all available data (see description below) covering the location of the transient. The left panel of Figure 1 shows the

[14] Although M85 2006OT-1 is observationally similar to other LRNe, its nature is more controversial: Kulkarni et al. (2007) (see also Ofek et al. 2008; Rau et al. 2008) supported the idea of a low-to-moderate mass merger, while Pastorello et al. (2007) favored the weak core-collapse supernovae (CCSNe) explosion scenario.

[15] http://www.cbat.eps.harvard.edu/unconf/followups/J14021678+5426205.html

[16] The NASA/IPAC Extragalactic Database (NED) is operated by the Jet Propulsion Laboratory, California Institute of Technology, under contract with NASA.

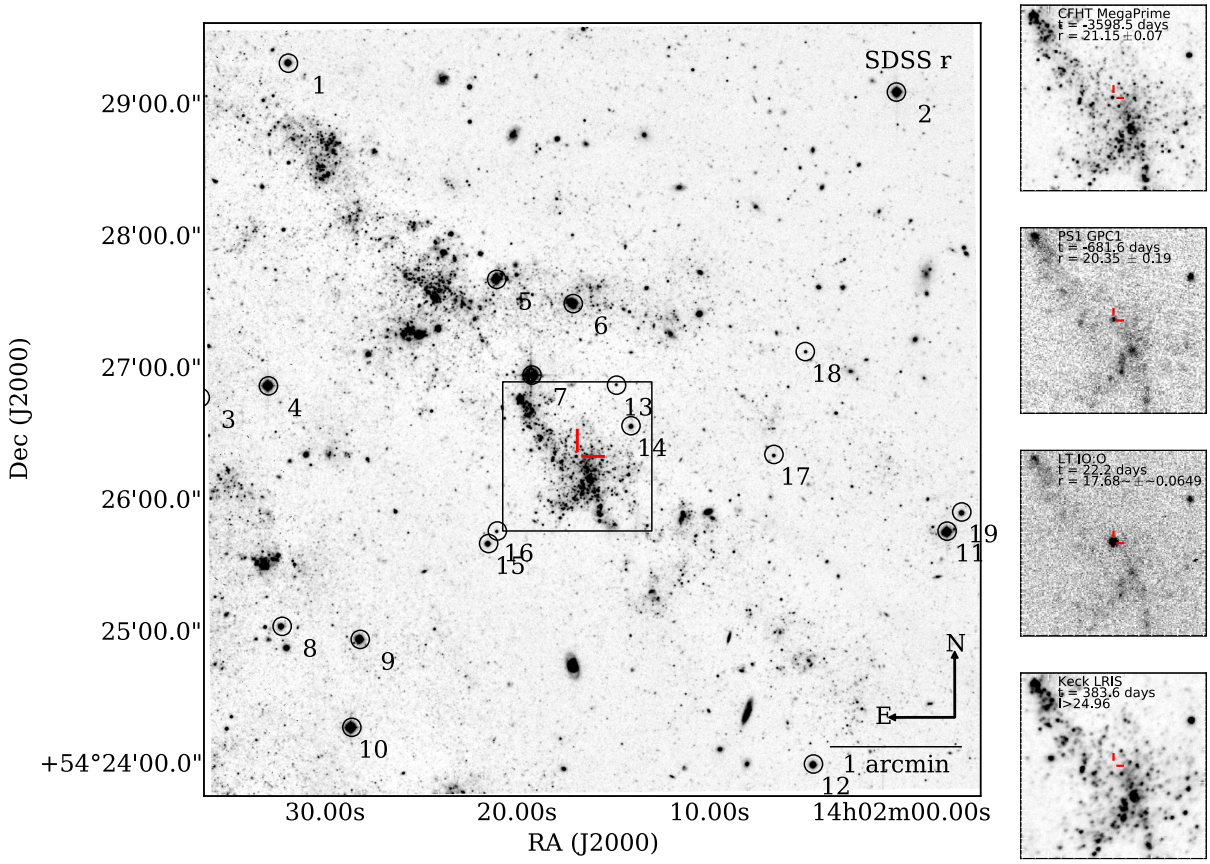

Figure 1. Left: M101-OT and the reference stars used to calibrate the photometric zero-point. Due to a variable field of view, position, and position angle for the M101-OT historical photometric images, different subsets of the fields stars were used according to their visibility. At any time, a minimum number of three stars was used. The square region around M101-OT is shown in detail on the right-hand side. Right: images of M101-OT at four epochs: ≈10 years before the reference epoch, 22.3 months, 22 days after the second outburst, and 12.6 months after. The field-of-view size is $1' \times 1'$ centered on the position of M101-OT. The red dashes show the location of the transient. The telescope, instrument, and magnitude of the object are listed for each image.

location of M101-OT and reference stars used for calibration. The right panel shows the magnitude evolution for −10 years, −1.8 years and an early followup epoch at 22 days after the second peak. The source has faded below detectable limits at +383 days. Throughout this work, we will use as a reference epoch the date of the second peak in *r*-band, MJD 57070.

Our best quality pre-discovery image (seeing of 0.″55) is an *r*-band exposure at −3625 days pre-peak from the Canada–France–Hawaii Telescope (CFHT). We aligned this image with our +22-d post-peak image using 18 stars in common. There is one point source (see right-hand side of Figure 1) in the image within a 2″ radius of the position during the outburst, and the central position of the point-spread functions (PSFs) are coincident within 180 mas (with a precision in the alignment of 250 mas). We identify this point source as the progenitor of M101-OT. Imaging in *I*-band taken at late times with Keck confirm the disappearance of the progenitor star.

The historical optical data for M101-OT was retrieved from the CFHT MegaPrime and CFHT12K/Mosaic, using single and combined exposures (Gwyn 2008), Pan-STARRS-1/GPC1 (Schlafly et al. 2012; Tonry et al. 2012; Magnier et al. 2013, PS1;), Isaac Newton Telescope/Wide Field Camera (INT/WFC), and Sloan Digital Sky Survey (SDSS) DR 10 (Ahn et al. 2014). Unfortunately, there are no *HST* images covering the location of the source. Post-discovery optical magnitudes were obtained from the reported followup astronomer's telegrams (ATels), Liverpool Telescope (LT), the Nordic Optical Telescope (NOT), and the Palomar P48 and P60 telescopes. The infrared data were retrieved from CFHT/WIRCam, UKIRT/WFCAM, and the Spitzer Infrared Array Camera (Fazio et al. 2004) in 3.6 and 4.5 μm as part of the SPitzer InfraRed Intensive Transients Survey (SPIRITS) (M. M. Kasliwal et al. 2016, in preparation). Details of pre-discovery photometry and post-discovery optical photometry may be found in the Appendices Tables 1 and 2, respectively. iPTF photometry is reported in Table 3. The NIR and MIR observations are summarized in Appendix Table 5.

We measured the brightness of the source coincident with M101-OT using the IRAF SNOoPY[17] package for PSF photometry. The zero-point in the SDSS photometric system was calibrated using aperture photometry on three to nineteen different sequence stars in the M101-OT field. Figure 1 shows the position of the sequence stars. Their coordinates and magnitudes are reported in Table 4. The magnitude measurements for bands *grizy* were obtained from the PS1 catalog, having photometric accuracy better than 0.01 mag. Measurements for *u*-band were obtained from the SDSS DR10 catalog. Johnson photometry was calibrated using the same PS1 catalog and transformations provided by Tonry et al. (2012) with an

[17] SNOoPY is a package developed by E. Cappellaro, based on DAOPHOT, but optimized for SN magnitude measurements.

Table 1
Historic Photometric Measurements of M101-OT

Phase (days)	MJD (+50000)	Tel.	m_U (mag)	m_B (mag)	m_V (mag)	m_R (mag)	m_u (mag)	m_g (mag)	m_r (mag)	m_i (mag)	m_z (mag)	m_y (mag)	Unfilt. (mag)	References
−5413.5	1656.5	CFHT	⋯	21.94 ± 0.11	21.89 ± 0.31	21.16 ± 0.19	⋯	⋯	⋯	⋯	⋯	⋯	⋯	⋯
−5410.8	1659.2	INT	⋯	⋯	⋯	⋯	⋯	⋯	21.17 ± 0.17	⋯	⋯	⋯	⋯	⋯
−4364.0	2706.0	SDSS	⋯	⋯	⋯	⋯	23.13 ± 0.49	21.79 ± 0.09	21.86 ± 0.14	21.31 ± 0.08	21.94 ± 0.58	⋯	⋯	(1)
−3920.1	3149.9	INT	⋯	21.83 ± 0.22	⋯	⋯	⋯	⋯	⋯	⋯	⋯	⋯	⋯	⋯
−3860.6	3209.4	CFHT	⋯	⋯	⋯	⋯	21.82 ± 0.36	21.38 ± 0.13	⋯	⋯	⋯	⋯	⋯	⋯

Note. Reference: (1), Kelly et al. (2015).

(This table is available in its entirety in machine-readable form.)

Table 2
Post-discovery Photometric Measurements of M101-OT

Phase (days)	MJD (+50000)	Tel.	m_U (mag)	m_B (mag)	m_V (mag)	m_R (mag)	m_I (mag)	m_u (mag)	m_g (mag)	m_r (mag)	m_i (mag)	m_z (mag)	Refs.
4.0	7074.0	SAI−2.5 m	⋯	19.09 ± 0.02	17.71 ± 0.02	16.83 ± 0.02	⋯	⋯	⋯	⋯	⋯	⋯	(1)
7.9	7077.9	SAO−6 m	⋯	19.04 ± 0.02	17.69 ± 0.02	16.83 ± 0.02	⋯	⋯	⋯	⋯	⋯	⋯	(1)
11.1	7081.1	SAI−2.5 m	⋯	19.23 ± 0.02	17.79 ± 0.02	16.90 ± 0.02	⋯	⋯	⋯	⋯	⋯	⋯	(1)
17.1	7087.1	NOT	⋯	19.57 ± 0.05	18.12 ± 0.02	17.07 ± 0.01	16.35 ± 0.05	⋯	⋯	⋯	⋯	⋯	⋯
22.2	7092.2	LT	⋯	19.90 ± 0.26	⋯	⋯	⋯	⋯	19.06 ± 0.20	17.73 ± 0.06	17.23 ± 0.08	16.88 ± 0.07	⋯

Note. Reference: (1) Goranskij et al. (2015).

(This table is available in its entirety in machine-readable form.)

Table 3
iPTF Followup Data of M101-OT

Phase (days)	MJD (+50000)	Telescope	m_g (mag)	m_r (mag)	m_i (mag)
−2005.8	5064.2	PTFP48	⋯	20.26 ± 0.11	⋯
−1706.7	5363.3	PTFP48	⋯	20.31 ± 0.11	⋯
−1682.7	5387.3	PTFP48	⋯	20.18 ± 0.15	⋯
−1484.6	5585.4	PTFP48	⋯	20.17 ± 0.13	⋯
−1345.7	5724.3	PTFP48	⋯	20.25 ± 0.14	⋯

Note. The errors are given in brackets.

(This table is available in its entirety in machine-readable form.)

rms below 0.1 mag. Photometry from the iPTF survey was obtained with the Palomar Transient Factory Image Differencing Extraction (PTFIDE) pipeline for the 48 inch telescope (Masci et al. 2016) and with a custom difference imaging pipeline for the 60 inch telescope at Mount Palomar (Cenko et al. 2006). Transformations from PTF Mould-*R* and *g*-band to SDSS equivalent photometry were obtained using the transformations in Ofek et al. (2012). The NOT NIR reductions were based on using an external IRAF package NOTCAM VERSION 2.5[18] and a custom pipeline for WIRC data. The zero-point for IR photometry was calibrated using the Two Micron All Sky Survey (2MASS) photometry.

The full historical light curve of M101-OT is shown in Figure 2, left panel. The earliest detection of the progenitor was obtained on 2000 February 05 with CFHT. From these first single-epoch observations, we get $B = 21.9 \pm 0.1$, $V = 21.8 \pm 0.3$, $R = 21.1 \pm 0.2$ (corrected for Milky Way extinction), which at the distance of M101 yield absolute magnitudes of $M_B = -7.1$, $M_V = -7.2$, and $M_R = -7.9$ for the progenitor star. INT observations in the *r*-band, $r = 21.2 \pm 0.15$, taken only three days after CFHT, are consistent within 0.1 mag with the *R*-band measurements.

Within the first period, from approximately 15–5.5 years before the outburst, the brightness of the progenitor shows only minor variations. The magnitude in the *r*-band remained constant to within 0.2 mags, with an average value of $r = 21.1$. Roughly 5.5 years before the outburst, the light curve began to rise smoothly across all bands. The *r*-band increased to 19.6 mag at −180 days, i.e., 1.5 mag relative to the historical median value. Reported magnitudes prior to mid-2012 (−2.7 years) taken with the Large Binocular Telescope (LBT) agree with these values: the source was reported as being variable, with mean magnitudes of $U = 21.33 \pm 0.19$, $B = 21.30 \pm 0.19$, $V = 20.97 \pm 0.17$, and $R = 20.69 \pm 0.17$ (Gerke et al. 2015). During its slow rise, the transient was detected on 2013 April 04 (−684 days) internally by iPTF as a slowly brightening source.

On 2014 November 10, after appearing from behind the Sun, it was detected at 16.6 mag in R-band during its first outburst (Cao et al. 2015), ∼3 months prior to public discovery. At approximately −29 days to peak, it was also detected by LBT in between the first and second outbursts at a considerably fainter magnitude of $R = 18.22 \pm 0.02$ (Gerke et al. 2015). At the time of the public announcement on 2015 February 10, the object was close to its second peak, estimated to fall 10 days later, on 2015 February 17 (MJD 57070).

[18] http://www.not.iac.es/instruments/notcam/guide/observe.html

The *Gaia* satellite (Perryman et al. 2001) (a European Space Agency mission) serendipitously observed the region containing M101-OT during the time of the first peak. Unfortunately, these data have not been made available to us. Due to this handicap in constraining the time of the first peak, we choose to adopt the epoch of maximum brightness of the second peak, at MJD 57070, as our reference epoch.

The followup photometry for M101-OT is shown in the right panel of Figure 2. The most remarkable feature of the light curve is the existence of two maxima. The object was observed during the decay phase of the first peak, having an absolute magnitude of $M_r \leqslant -12.6$ mag (we only have data on the decline part for the first peak, and so the outburst could have been brighter). The second maximum, ∼100 days after it shows $M_r \simeq -12.0$ mag and is followed by a fast-declining phase, lasting ∼40 days, when the object fades 2 magnitudes in *r*-band. The light curve makes a transition into a plateau phase of ∼60 days: the redder riz bands flatten, while the bluer *Bg*-bands continue to decline. After the end of the plateau, around +110 days, the transient resumes the initial decline rate in *r*-band. The first NIR followup data show magnitudes of $J = 15.45 \pm 0.3$, $H = 15.07 \pm 0.06$, and $K = 14.94 \pm 0.09$ at +17 days. The evolution in the IR bands is slow, and only after day +200 the object starts to decline in the IR too. Between +200 and +256 days it fades by ∼1 mag in the *K*-band. However, later epoch observations provided by (Goranskij et al. 2015) and followup with P200 and NOT, suggest a rebrightening of the object in IR bands. Multiband photometry allows us to derive the blackbody temperature and radius of the object, shown in Figure 3 (see 3.2 for details).

The color evolution between −29 and +272 d for M101-OT is shown in Figure 4. Coincident with the end of the first phase of the light curve, at ∼50 days, the object becomes slightly bluer in *B* and *g*-bands. This period is associated with a decrease of the photospheric radius. At approximately +130 days, around the end of the plateau, the color evolution shows a second temporary (∼20 days) enhancement of flux ratio for the blue bands. The last multiband epoch (+154 days) shows that the object becomes increasingly red, i.e., $g - r = 1.9 \pm 0.4$, $g - z = 3.8 \pm 0.4$, and $V - K = 5.6 \pm 0.2$.

2.2. Optical Spectroscopy

We obtained spectra of M101-OT using a range of facilities. The log of the spectroscopic observations is given in Table 6. The data were reduced using IRAF and PyRAF standard routines. The wavelength calibration was done by fitting low-order polynomials to arc lamp spectra. Sky lines were used to check the accuracy of the calibration, which is within 1 Å. We calibrated the flux using spectrophotometric standard stars and later on we adjusted it using interpolated photometry for the same epoch as the spectra. The spectra of M101-OT are made public via WISeREP (Yaron & Gal-Yam 2012).

We assumed the heliocentric recessional velocity for M101 of 241 ± 2 km s^{-1} (de Vaucouleurs et al. 1991). Figure 5 shows the spectral evolution of M101-OT. All spectra show a cool photospheric continuum, fitted by a blackbody emission with temperatures of 3000–3600 K.

The blue part of the M101-OT spectrum is dominated by the absorption forest of Fe II (at around 5400 Å), Ti II (below 4700 Å), and Sc II lines. P-Cygni profiles are displayed by intermediate-mass elements. Ca II is identified with an expansion velocity of $v \simeq -356 \pm 9$ km s^{-1} for the absorption

Table 4
Sequence Star Magnitudes used for the M101 Field

Star #	α (J2000.0)	δ (J2000.0)	m_g (mag)	m_r (mag)	m_i (mag)	m_z (mag)	m_y
1	210.6328	54.4887	18.347 (0.007)	17.488 (0.004)	17.123 (0.004)	16.935 (0.006)	16.836 (0.007)
2	210.5005	54.4851	17.463 (0.005)	16.388 (0.005)	15.776 (0.004)	15.498 (0.004)	15.357 (0.004)
3	210.6519	54.4464	16.426 (0.004)	15.692 (0.004)	15.398 (0.004)	15.277 (0.004)	15.190 (0.005)
4	210.6370	54.4479	16.863 (0.006)	15.915 (0.005)	15.534 (0.005)	15.359 (0.003)	15.251 (0.006)
5	210.5874	54.4614	17.171 (0.007)	16.394 (0.005)	16.097 (0.005)	15.954 (0.003)	15.872 (0.005)
6	210.5708	54.4583	17.300 (0.007)	16.263 (0.004)	15.806 (0.004)	15.580 (0.004)	15.457 (0.005)
7	210.5798	54.4493	15.396 (0.005)	14.510 (0.004)	14.128 (0.004)	13.940 (0.003)	13.830 (0.004)
8	210.6340	54.4175	19.256 (0.012)	18.031 (0.006)	17.273 (0.004)	16.915 (0.005)	16.745 (0.008)
9	210.6171	54.4159	17.990 (0.011)	16.725 (0.004)	15.850 (0.005)	15.444 (0.003)	15.242 (0.005)
10	210.6189	54.4048	16.238 (0.004)	15.794 (0.003)	15.631 (0.003)	15.577 (0.003)	15.547 (0.005)
11	210.4896	54.4296	16.789 (0.011)	16.347 (0.004)	16.250 (0.004)	16.183 (0.004)	16.172 (0.007)
12	210.5186	54.4001	18.317 (0.007)	17.516 (0.004)	17.191 (0.005)	17.012 (0.006)	16.901 (0.007)
13	210.5614	54.4480	21.791 (0.110)	21.516 (0.062)	21.341 (0.060)	20.938 (0.205)	...
14	210.5582	54.4429	19.752 (0.022)	19.292 (0.010)	19.133 (0.010)	19.080 (0.017)	18.984 (0.039)
15	210.5892	54.4280	19.388 (0.012)	18.499 (0.007)	18.187 (0.005)	18.024 (0.008)	17.918 (0.018)
16	210.5873	54.4296	22.027 (0.185)	21.018 (0.051)	19.627 (0.013)	19.041 (0.018)	18.646 (0.028)
17	210.5272	54.4393	21.070 (0.036)	20.555 (0.028)	20.313 (0.022)	20.209 (0.041)	19.641 (0.107)
18	210.5204	54.4523	21.392 (0.048)	21.017 (0.039)	20.799 (0.034)	20.758 (0.072)	...
19	210.4864	54.4320	19.935 (0.017)	18.712 (0.007)	17.673 (0.004)	17.199 (0.005)	16.962 (0.010)

Note. The values are computed from the stacked magnitudes from Pan-STARRS. The errors are given in brackets. Coordinates and magnitudes are taken from the Pan-STARRS PV2 Catalog.

component at +2 days, slowing to $v \simeq -283 \pm 2$ km s^{-1} at +22 days, and $v \simeq -207 \pm 17$ km s^{-1} at +116 days. Ba II $\lambda\lambda$ 6134, 6489 is also identified as P-Cygni profile with an expansion velocity of -180 km s^{-1} and a FWHM of 367 km s^{-1}. Other elements present in early-time spectra are λ 5150 Mg and Na I at $\lambda\lambda$ 5890, 5896 and $\lambda\lambda$ 8183, 8195. Resonance lines K I $\lambda\lambda$ 7665, 7699 and $\lambda\lambda$ 7665, 7699 are also found in the spectrum, although their P-Cygni profiles are much weaker. These lines are rare and have been seen in the extreme supergiant VY CMa (Smith 2004) and Type IIn SN 2009kn (Kankare et al. 2012). We do not detect strong [Ca II] $\lambda\lambda$ 7291, 7325 lines in the spectrum, which have been associated with dense and compact gas disk and presence of dust (Smith et al. 2010; Liermann et al. 2014). Figure 5 shows comparison spectra for similar red transients. M85-OT2006-1 is defined as an SN2008S-like observational class, showing strong emission for CaII and [Ca II] lines. UGC2773-OT2009-1 is considered to be an example of a dust-enshrouded luminous blue variable (LBV). NGC4490-OT2011-1 and V838 Mon are examples of LRNe. There is an important resemblance between all three groups, implying that the nature of the outburst cannot be determined from spectra alone.

The spectra of M101-OT have a significant evolution of the Hα profile. Figure 6 shows different morphologies of the profiles for different epochs. At early times, its expansion velocity, derived from the FWHM, is around 500 km s^{-1}, slightly larger than the one of intermediate-mass elements. The profile is asymmetric and shows a small blueshifted absorption component. However, at +22.9 days the absorption evolves into an emission profile, suggesting the existence of asymmetry in the outflow. The implications of this are further discussed in Section 3.1.1. Similar behavior was observed in the high-resolution spectra of NGC4490-OT2011-1 reported in Smith et al. (2016b).

3. ANALYSIS

3.1. Spectroscopic Analysis

3.1.1. The Hα profile

An interesting feature is the evolution to a double-peaked profile of the Hα line (Figure 6). There is evidence for a double-peaked line, with a difference in velocity of ~500 km s^{-1} between the components. Spectra taken around the peak show the blueshifted P-Cygni component in absorption.

However, for later epochs, after the beginning of the plateau phase at +40 days, the absorption disappears and an increasingly bright blueshifted emission peak appears instead. The second emission component becomes clearly visible at +54 days, and reaches a similar equivalent width as the redshifted counterpart at +116 days.

Similar absorption in the blue wing evolving into an emission component was also observed for the LRNe V1309 Sco (Mason et al. 2010) and NGC 4490 2011OT-1 (Smith et al. 2016b), which both had higher spectral resolution data.

3.1.2. Molecular Bands

Spectra taken at +116 days and later epochs show the initial formation of molecular bands, characteristic of cool M-type stars. Figure 7 shows the comparison between M101-OT spectrum at +154 days, with a cool M5III star and the UVES/VLT average spectrum of V838 Mon taken in 2009 January, February, and March, about seven years after the outburst (Tylenda et al. 2011). Although the resolution of the GTC spectrum is not high enough (380 km s^{-1}) to resolve individual bands, they match well with a spectrum of an M5III star (Bagnulo et al. 2003). At this phase, the photospheric temperature shows a good fit with the ~3000 K blackbody. We detect titanium oxide (TiO) bands in the range 6600–6800 Å and 7050–7300 Å. Between 7300 and 7600 Å,

Table 5
NIR and MIR Photometry of M101-OT

Phase (days)	MJD (+50000)	Telescope	J (mag)	H (mag)	K (mag)	3.6 μm (mag)	4.5 μm (mag)
−4065.0	3005.0	Spitzer	⋯	⋯	⋯	19.00 ± 0.01	18.60 ± 0.01
−3997.5	3072.5	Spitzer	⋯	⋯	⋯	⋯	>20.48
−2075.0	4995.0	CFHT	22.74 ± 0.53	⋯	19.54 ± 0.11	⋯	⋯
−1756.6	5313.4	UKIRT	20.61 ± 0.16	⋯	⋯	⋯	⋯
17.1	7087.1	NOT	15.48 ± 0.03	15.10 ± 0.06	14.97 ± 0.09	⋯	⋯
48.0	7118.0	NOT	16.42 ± 0.03	15.74 ± 0.05	15.47 ± 0.01	⋯	⋯
62.6	7132.6	Spitzer	⋯	⋯	⋯	14.72 ± 0.01	14.75 ± 0.01
74.0	7144.0	NOT	16.70 ± 0.04	15.72 ± 0.02	15.49 ± 0.07	⋯	⋯
90.3	7160.3	Spitzer	⋯	⋯	⋯	14.55 ± 0.01	14.59 ± 0.01
102.0	7172.0	NOT	16.63 ± 0.03	15.90 ± 0.04	15.41 ± 0.06	⋯	⋯
121.8	7191.8	Spitzer	⋯	⋯	⋯	14.50 ± 0.01	⋯
136.0	7206.0	NOT	16.53 ± 0.02	16.01 ± 0.03	15.46 ± 0.04	⋯	⋯
150.8	7220.8	Spitzer	⋯	⋯	⋯	14.39 ± 0.01	⋯
197.9	7267.9	NOT	17.16 ± 0.03	16.02 ± 0.03	15.25 ± 0.02	⋯	⋯
202.7	7272.7	Spitzer	⋯	⋯	⋯	14.30 ± 0.01	14.50 ± 0.01
253.3	7323.3	NOT	⋯	17.87 ± 0.07	16.32 ± 0.03	⋯	⋯
280.3	7350.3	NOT	⋯	>16.56	16.81 ± 0.07	⋯	⋯
339.0	7409.0	SAI-2.5m	18.65 ± 0.05	17.64 ± 0.10	16.32 ± 0.05	⋯	⋯
385.0	7455.0	SAI-2.5m	21.00 ± 0.20	20.20 ± 0.30	18.20 ± 0.20	⋯	⋯
403.4	7473.4	P200	21.85 ± 0.42	19.59 ± 0.17	17.91 ± 0.12	⋯	⋯
438.0	7508.0	NOT	⋯	⋯	17.22 ± 0.12	⋯	⋯
514.0	7584.0	NOT	20.01 ± 0.24	18.77 ± 0.13	17.25 ± 0.13	⋯	⋯

TiO absorption is combined with vanadium oxide (VO) molecular absorption, which becomes dominant above 7400 Å.

3.2. Spectral Energy Distribution (SED) Analysis and Bolometric Light Curve

We computed a blackbody fit to several pre- and post-discovery epochs, preferentially taken around the same epoch, or at most ±50 days from each other. In the case where a particular band had more than one measurement within the time interval, we computed the mean value weighted by the errors.

We used the Markov Chain Monte Carlo PYTHON package EMCEE (Foreman-Mackey et al. 2013) to obtain the value of the maximum posterior probability and 1σ confidence intervals on the estimated parameters. The evolution of temperature and radius for the best blackbody fit is shown in Figure 3. In all cases, a single blackbody component was sufficient to describe the observed SED.

The initial fits for the progenitor at epochs earlier than 6 years, show that the temperature and radius were constant within the errors with values of $T = 6600 \pm 300$ K and an $R = 220 \pm 25$ $R_\odot$. Starting at −5.5 years, there was a progressive expansion and cooling of the star, so that at −250 days it cooled down to $T = 5800 \pm 120$ K and nearly tripled its radius to $R = 620 \pm 25$ $R_\odot$. During the peak of the second outburst, the temperature had decreased to roughly 3300 K, and continued to cool down slowly over the next 400 days. The photospheric radius showed a peculiar behavior. It had grown exponentially up to $R \sim 6500 \pm 400$ $R_\odot$ during the outburst peak, receded to $R \sim 4300 \pm 80$ $R_\odot$ at 48 days and expanded again to approximately $R \sim 7800 \pm 50$ $R_\odot$ at 200 days. A similar effect was noted for M31 2015 LRN (MacLeod et al. 2016). We fitted a linear model for the radial expansion for epochs 70–200 days, which allowed us to derive the photospheric expansion velocity of 170 ± 5 km s^{-1}.

Around the second outburst, from 10–30 days, the temperature had a constant value of 3670 ± 50 K. The plateau phase, detected in the redder bands, is associated with a slower decline in the temperature: ≃150 K between days 40 and 100. IR photometry for later epochs (>400) show that the temperature is consistent with 1200 ± 300 K blackbody emission.

The integrated blackbody emission was used to estimate the bolometric light curve for M101-OT, as shown in Figure 8. While the early-time photometry shows a rather stable object with luminosity $L \simeq 2.6 \times 10^5$ $L_\odot$, photometry later than five years prior to the outburst shows a steady increase in the star's bolometric luminosity, reaching $L \sim 4 \times 10^5$ $L_\odot$ at 250 days before and approximately $L \simeq 6.3 \times 10^6$ $L_\odot$ during the maximum of the second outburst.

3.3. Progenitor Analysis

3.3.1. Single Star Scenario

Photometric measurements from the earliest three archival epochs, obtained between 15 and 8 years before the outburst, were used to derive the best parameters for the progenitor star. We found a good agreement with a single blackbody fit. No significant IR excess was observed in the early photometric measurements. The star was estimated to have a temperature of $T = 6600 \pm 300$ K and an approximate radius of $R = 220 \pm 13$ $R_\odot$. The historic average bolometric luminosity is $L \sim 8.8 \pm 0.8 \times 10^4$ $L_\odot$, which placed the progenitor star to be below the low-luminosity end of the LBV zone in the HR diagram (Smith et al. 2004), where known LBVs tend to have luminosities greater than $L \sim 2 \times 10^5$ $L_\odot$.

In order to derive the characteristics of the progenitor system, we compared (using maximum likelihood) the observed broadband photometric archival measurements with

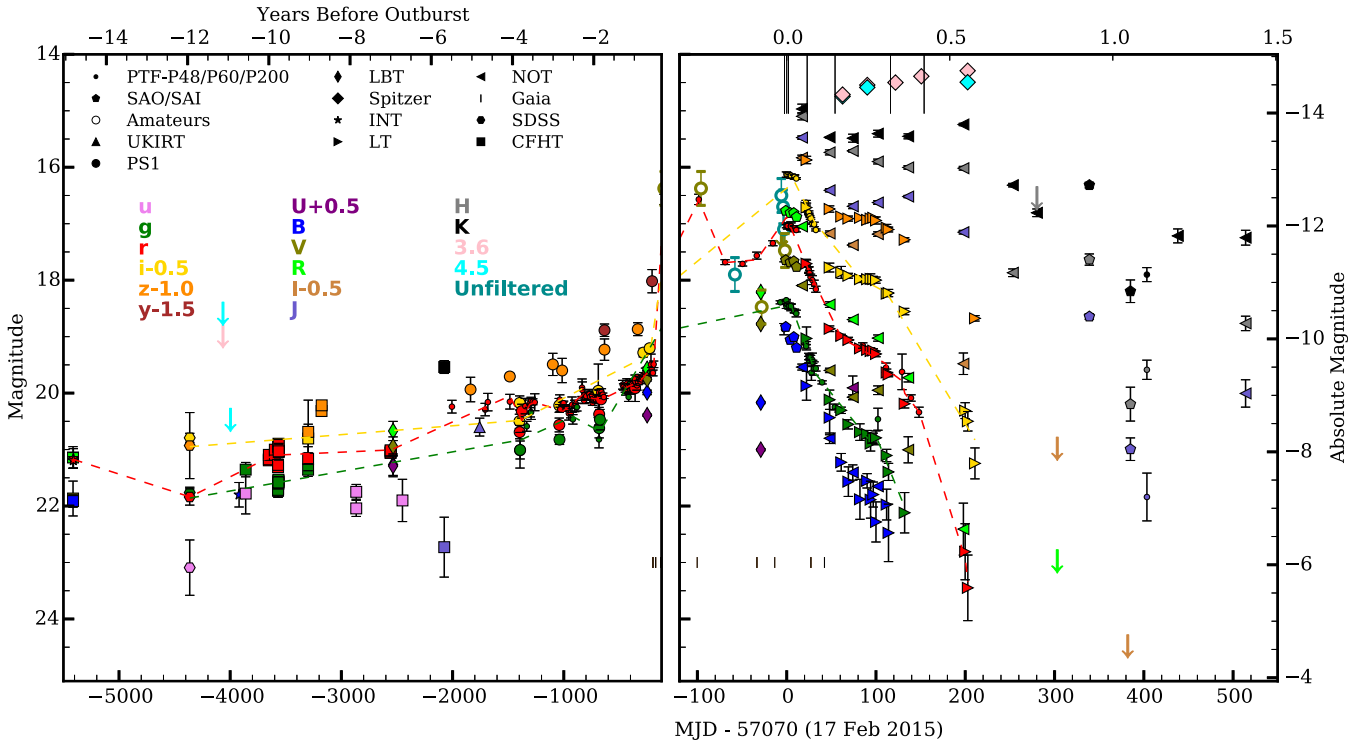

Figure 2. Left: historic light curve for M101-OT spanning fifteen years of observations until 120 days before the second peak date. Pan-STARRS1 and iPTF data allow us to note an increase in the baseline magnitude of the transient at about 5.5 years before the eruption. Dashed lines are used to guide the eye. Downward-pointing arrows indicate upper limits. Right: close up of the light curve from −120 days to +550 days after the outburst. For each data point, the marker shape shows the telescope and the color indicates the filter. Note the difference in timescale between the left- and right-hand side plots. Vertical tickmarks below the light curve show the epochs when this object was observed by *Gaia* (still proprietary data). Upper vertical lines show the epochs when spectra were taken. The light curve shows two maxima at ∼−100 and 0 days.

the predicted absolute magnitudes in the BPASS models.[19] Specifically, we obtained the averaged photometric measurements over all epochs older than −5.5 years to compare them with the predicted photometry of the system for both single and binary stellar models. Single-star evolution tracks were taken from BPASS v1.0 (Eldridge & Tout 2004) and binary stellar evolution tracks from BPASS v2.0 (Stanway et al. 2016). We assumed solar metallicity for both cases.

For the case of a single-star evolution scenario with fixed metallicity, the only free parameter of the model is the initial progenitor mass. Figure 9 shows the location of the progenitor star in the temperature-luminosity space for three historic measurements. The progenitor star is consistent with an F-type yellow supergiant, with initial mass of 18–19 $M_{\odot}$, that is evolving off the main sequence toward the red supergiant phase. The location of the progenitor, named the Hertzsprung gap, is extremely unusual, as it is associated with stars that have finished core hydrogen burning, but have not yet started the shell hydrogen burning phase. Stars are expected to spend only a small fraction of their lives (∼3000 years) in the region where the progenitor system is found, as shown in Figure 9. Stars in the gap experience an exponential increase in the stellar radius, from ∼20 $R_{\odot}$ to ∼800 $R_{\odot}$ for a 18 $M_{\odot}$ star. The age of the star is when the progenitor reaches 230 $R_{\odot}$ and is 9.9 ± 0.1 Myr.

3.3.2. Binary Star Scenario

Detailed modeling of the event assuming a binary star evolution scenario is beyond the scope of this paper. In the current work, we aim to provide initial constraints on the progenitor system and the possible fate of the remnant.

We define the common envelope (CE) evolution as a short-lived phase in the evolution of an interacting binary system (Paczynski 1976). It is initiated when the most evolved star expands enough to overfill its Roche lobe (RL), triggering an unstable mass transfer toward its companion, which accumulates in a CE surrounding both stars (see Ivanova et al. (2013b) for a review). The RL radius for the primary star is well approximated by Eggleton (1983).

$$RL_1 = a\frac{0.49q^{2/3}}{0.6q^{2/3} + \ln(1+q^{1/3})} \quad (1)$$

where $q = M1/M2$ is the mass ratio where $M1$ is the mass of the primary, more massive star, and $M2$ is the mass of the secondary; a is the separation between the two components. We assume that the stars are in circular orbit and that the expansion of the primary takes place on a longer timescale than the formation of a CE. Therefore, during the stable phase before the outburst, the radius of the primary will be equivalent to its RL radius ($R1 = RL1$). From our observables, we estimate the radius for the primary star to be $R \simeq 230$ $R_{\odot}$. Under the condition of RL overflow, we can constrain the initial orbital separation a_i for different mass ratios of the system. For example, for a system with nearly equal masses and $q \simeq 1$, this value approximates to ≈600 $R_{\odot}$ and for $q = 18$ ($M1 = 18$ $M_{\odot}$ and $M2 = 1$ $M_{\odot}$), to ≈370 $R_{\odot}$. The periods associated to these separations are ≈290 and ≈190 days, respectively.

[19] http://bpass.auckland.ac.nz

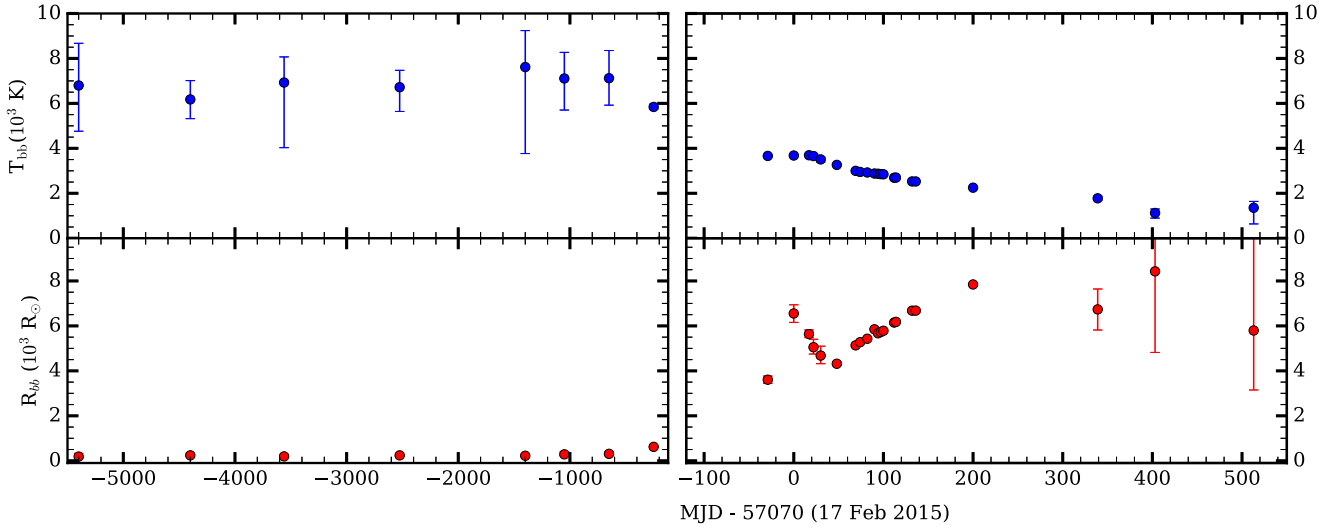

Figure 3. Left: evolution of the blackbody temperature and radius for M101-OT derived from photometry fits for the same time span as the light curve. We refer to the analysis in Section 3. Right: zoom from −120 to +550 days.

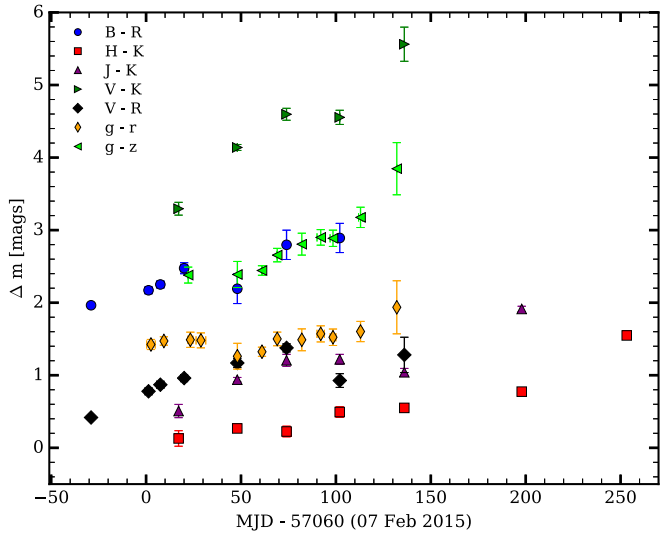

Figure 4. Post-outburst color evolution for M101-OT. The data points have been binned in groups of 10 days. The abscissa is the average MJD of the bin relative to the reference epoch.

The outcome of the CE phase can be expressed following the basic energy formalism (de Kool 1990; Ivanova et al. 2013b):

$$G\frac{M1M1_{\rm env}}{\lambda {\rm R1}} = \alpha_{\rm CE}\left(-G\frac{M1M2}{2a_i} + G\frac{M1_{\rm c}M2}{2a_f}\right). \quad (2)$$

The left side of the equation describes the binding energy of the envelope in the primary star. The right side describes the orbital energy released by the system from its initial orbital separation a_i, to its final separation a_f after the loss of the envelope. G is the gravitational constant, $M1_{\rm env}$ is the mass of the expelled envelope and $M1_{\rm c}$ is the mass of the remaining core. The parameter λ is related to the internal envelope structure of the star, and $\alpha_{\rm CE}$ represents the fraction of the gravitational binding energy that is used to eject the envelope with velocities larger than the local escape velocity. We assume $\lambda = 0.5$ (de Kool 1990) and $\alpha_{\rm CE}$ to be 0.5, which accounts for the need of kinetic energy of similar order of magnitude as the binding energy. According to the results derived from single stellar models, we fix $M1 = 18\ M_\odot$, $M1_{\rm env} = 13\ M_\odot$, and $M1_{\rm c} = 5\ M_\odot$. The estimated binding energy for the envelope when the radius of the primary is $R1 = 230\ R_\odot$ is of the order of $E_{\rm bind} \sim 8 \times 10^{48}$ erg. In order to be able to eject this envelope completely, the release of orbital energy needs to be equal to, or larger than $E_{\rm bind}$. Figure 10 shows the parameter space for the mass of the secondary component and the final orbital separation, which satisfies the energy balance stated above. We find that, in order to eject the envelope completely, the final separation of the system would need to be of the order of the radius of the secondary star (assuming it has the same age as the primary). The *spiral-in* phase would continue until the final separation a_f has shrunk below the radius of the secondary, eventually leading to the merger of the system. The conclusions presented here are not sensitive to small variations in the mass of the primary ($\pm 1\ M_\odot$), the initial separation a_i, or the dimensionless parameters λ and $\alpha_{\rm CE}$, sometimes treated as *fudge* factor in binary population synthesis models. According to these simple calculations, a (nearly) full ejection of the envelope for M101-OT would lead the system to merge.

An alternative interpretation is provided by binary evolution codes. We have examined the evolution of possible progenitor systems predicted by the BPASS v2.0 binary evolution models. These models, assuming solar metallicity, have three main parameters: mass of the primary, system mass ratio, and the logarithm of the period. These parameters are sampled in steps of 1 $M_\odot$, 0.2, and 0.2 dex respectively. As before, we assumed an initial mass for the primary $M1 = 18 M_\odot$ and imposed the constraint on the mass ratio and periods derived earlier from the progenitor radius ($R1 = RL1$). In all cases, the models predicted a surviving binary system with large final separation for the system, in the range $260 \leqslant a_f \leqslant 290\ R_\odot$. The discrepancy with the basic energy formalism is likely to be caused by the simplicity of our initial approach, which omits additional sources of energy, such as the star's internal energy, the thermal energy of the gas, or the recombination energy. The inclusion of these terms may reduce the magnitude of the binding energy, allowing the binary to survive. We note that

Table 6
Log of Spectroscopic Observations of M101-OT

Phase[a] (days)	MJD (+50000)	Date	Telescope+Instrument	Grating/Grism	Dispersion (Å/pix)	Resolution[b] (km s^{-1})	Exposure (s)
−2.5	7067.5	2015 Feb 14.5	P200+DBSP	7500	1.52	500	900
−2.0	7068.0	2015 Feb 15	NOT+ALFOSC	Grism#4	3.0	733	1800
0.1	7070.1	2015 Feb 17.1	Copernico 1.82m+AFOSC	GR04	4.3	630	1800
1.5	7071.5	2015 Feb 18.5	P200+DBSP	158/7500	1.52	420	1800
2.1	7072.1	2015 Feb 19.1	Copernico 1.82m+AFOSC	GR04	4.3	690	1800
22.9	7092.9	2015 Mar 11.9	WHT+ISIS	R300B+R158R	0.86 + 1.8	320	2 × 600 + 2 × 600
54.2	7124.2	2015 Apr 13.2	NOT+ALFOSC	Grism#4	3.0	747	2700
116.1	7186.3	2015 Jun 13.3	WHT+ISIS	R158R	1.8	345	2 × 1800
153.9	7223.9	2015 Jul 20.9	GTC+OSIRIS	R1000B	2.1	380	2 × 1800.0

Notes.
[a] Days since second peak at MJD 57070.
[b] Measured using the FWHM of λ 5577 O I sky line.

the interpretation of these results is only a suggestion, and further analysis is needed to draw firmer conclusions.

4. DISCUSSION

The absolute magnitude for M101-OT with peaks at $M_r \leqslant -12.4$ and $M_r \simeq -12.0$ mag, and its red color, $g - r = 1.4$ mag during the secondary peak, places this event in the so-called "gap" region of the timescale-luminosity diagram between novae (−4 to −10 mag), and SNe (−15 to −22 mag). Photometrically, the double-peaked light curve of M101-OT and increasingly red color resembles the complex nature of the objects in the LRNe group, with different scaling. However, such behavior is also shown by an object interpreted as an SN impostor, such as SN Hunt 248, in NGC 5806 (Kankare et al. 2015; Mauerhan et al. 2015).

The lack of periodic microvariation in the light curve −15 to −5 years before the outburst suggests that, unlike in the case of Galactic merger V1309 Sco, where both binary components were detected, for M101-OT only the brightest star in the system was seen. The unusual location of the progenitor in the Hertzsprung gap supports the hypothesis that the star is quickly expanding after finishing the core H-burning phase. If such a star has a close companion, whenever it expands enough to overfill its RL, it will initiate the mass transfer toward the secondary, forming a CE surrounding the binary system, so that the accretor will become engulfed in the envelope of the donor star.

Given the low densities in the outer layers of the donor atmosphere, the initial drag on the secondary may not be noticeable on short timescales. However, the spiral-in phase will accelerate with the secondary orbiting in increasingly denser layers of the primary star, eventually leading either to the merger of the components or the ejection of the envelope of the primary star on dynamical timescales. The slow brightening in M101-OT before the detected outbursts could have been associated with these final stages. The existence of optically thick ejected material is confirmed by the quick color evolution of M101-OT in the blue bands.

The spectrum of M101-OT is dominated by Hα, Ca II, Ba II, Na II, and K I at low expansion velocities (∼300 km s^{-1}) and a forest of Ti II and Fe II absorption lines at short wavelengths. These characteristics are similar to other LRNe, such as V838 Mon, M31 LRN, or NGC 4490 2011OT-1. However, low expansion velocities are not exclusive to this class. Members of the LBVs and ILOT classes also show outflow velocities well below 1000 km s^{-1}. The double-peaked Hα emission profile, tracing the bipolar structure of the ejecta, has also been observed in the asymmetric outflows of LBVs (Smith et al. 2016a) and nebular phases of SNe IIn with bipolar circumstellar medium (CSM) (Smith et al. 2015; Andrews et al. 2016) or CCSNe, such as SN 1987A (Gröningsson et al. 2008). Newly formed dust within the ejecta is responsible for the extinction of optical and NIR light. The redshifted component undergoes greater absorption from the generated dust, and, therefore, the blue emission may become more dominant at late epochs (Bevan & Barlow 2016).

One distinctive feature of M101-OT is the prompt formation of molecular bands, which strengthens the hypothesis of newly formed dust. At +154 days the spectrum showed evidence of the formation of TiO and VO bands, comparable to the ones seen in LRNe V4332 Sgr (Martini et al. 1999; Kamiński et al. 2010) and V838 Mon (Rushton et al. 2005; Tylenda et al. 2011).

Possible interpretations of the true nature of M101-OT may include a wide range of scenarios. Some examples are: onset of the CE, similar to the one witnessed for M31 2015 LRN (MacLeod et al. 2016); mass loss during turbulent phases of the stellar evolution (e.g., during the post He-burning phase); mass-loss events triggered by the passage of a lower-mass companion to the periastron and the subsequent shell–shell collision in very eccentric orbits; swallowing of planets by an expanding red giant (Retter & Marom 2003); mass-transfer-induced jets, similar to the ones suggested for M31 2015 LRN and SN 2015bh (Soker 2016; Soker & Kashi 2016); a faint terminal explosion or even thermal emission from shocks originated from the mass loss in the binary system (Pejcha et al. 2016). The binary merger scenario proposed in this work, has also been presented by Goranskij et al. (2016), who interpreted M101-OT as the ejection of a common envelope and the merger of a massive OB binary system.

We argue that, within the context of binary evolution models, M101-OT likely represents the best-studied case of an unusual event of the ejection of the CE in a massive binary system. Detailed modeling is required to determine whether the two components survived in a closer orbit or merged completely. The characteristics of the M101-OT agree with the empirical correlation between the peak absolute magnitude

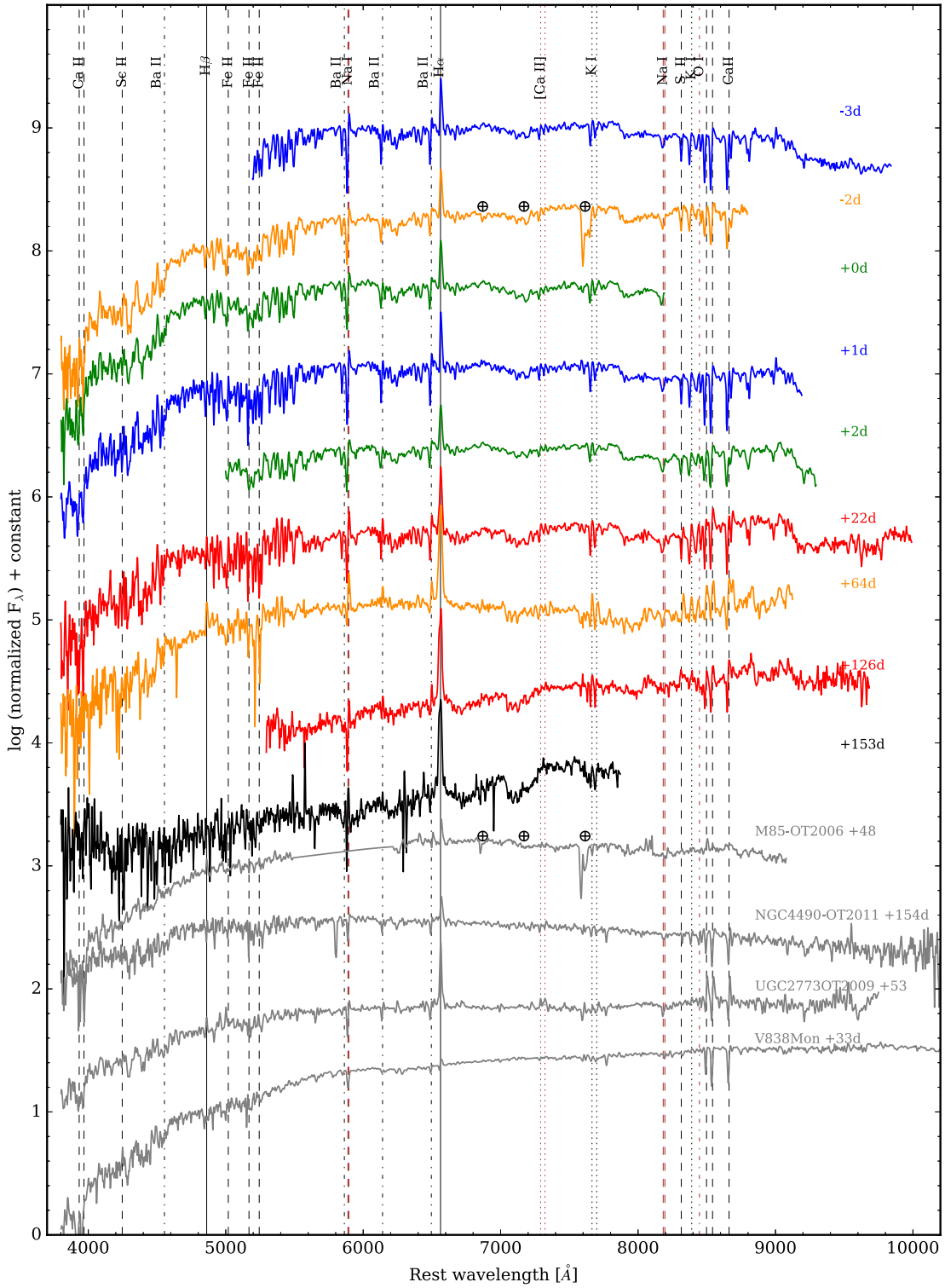

Figure 5. Spectral evolution of M101-OT. The spectra have been flux calibrated using the interpolated photometric measurements. Telluric absorption features were corrected or marked otherwise with a ⊕ symbol. Because the response of the detector drops at the extremes, some spectra are only shown for the valid wavelength range. The spectrum is color coded by instrument. Blue: P200+DPSP, green: 1.82m+AFOSC, red: WHT+ISIS, orange: NOT+ALFOSC, black: GTC+OSIRIS, gray: comparison spectra. The Keck/LRIS spectrum of M85-OT is from (Kulkarni et al. 2007), NGC 4490-OT from (Smith et al. 2016b), the UGC2773-OT2009 spectrum was taken with TNG/DOLORES (A. Pastorello 2016, private communication), and finally the spectrum of V838 Mon was taken with the Kast spectrograph at Lick Observatory on 2002 March 11 (Smith et al. 2016b).

in *I*-band and the progenitor mass suggested by Kochanek et al. (2014). Future surveys, such as the Zwicky Transient Facility (ZTF), targeting larger numbers of nearby galaxies would help to populate this correlation in the more massive end.

5. SUMMARY AND CONCLUSIONS

M101-OT is a transient with LRN characteristics discovered in a star-forming region in a spiral arm of M101. A summary of its most relevant observational characteristics is given below:

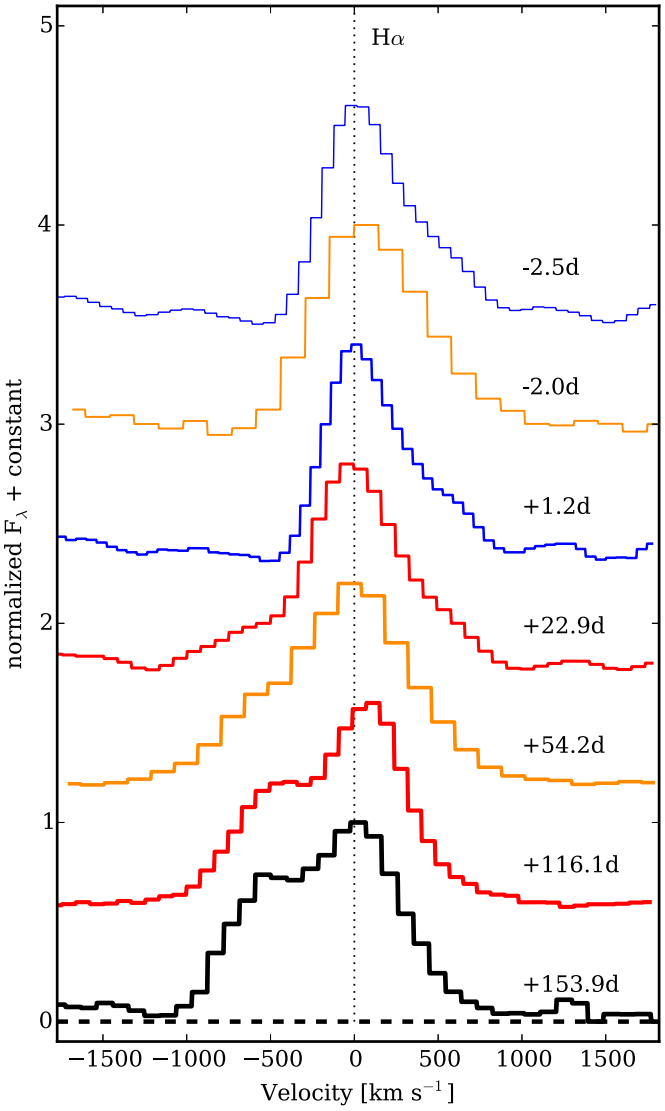

Figure 6. The continuum-subtracted and peak-normalized Hα region for DBSP (500 km s^{-1}), WHT (320 km s^{-1}), NOT (747 km s^{-1}) and GTC (380 km s^{-1}) spectra. The spectrum is color coded by instrument, the same as in Figure 5.

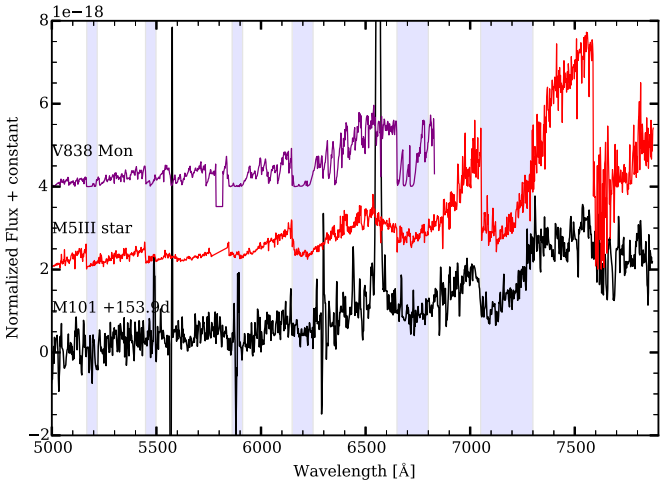

Figure 7. Comparison of M101-OT spectrum at +154 days with HD118767 M5III star (Bagnulo et al. 2003) and the average spectrum of V838 Mon (Tylenda et al. 2011). The spectrum has an estimated blackbody temperature of ∼3000 K. The molecular bands are comparable to the ones in cool giant stars. Major molecular absorption lines are marked in the spectrum with blue vertical bands.

1. The historic evolution of M101-OT shows no major variations within 0.2 mag in *R*-band until approximately 5.5 years before the outburst.
2. The pre-outburst SED suggests no IR excess, implying the lack of an old existing dust-emission component.
3. The object has slowly brightened by 1.5 mags over the last 6 years prior to the outburst. The estimated radius appeared to increase from 230 ± 13 $R_\odot$ at 6 years before the outburst, to 6500 $R_\odot$ during the secondary outburst maximum.
4. The light curve shows two peaks, detected in *R*-band, separated by ⩾ 100 days. The magnitude of the first peak is $M_r \leqslant -12.4$ mag (lower limit because of an observation gap) and $M_r \simeq -12.0$ during the second peak. The color of the object during the second maximum is $g - r = 1.4$ mag, which corresponds to an estimated temperature of 3600 K.
5. Late-time followup photometry suggests the rebrightening of the object in IR wavelengths after one year.
6. The bolometric luminosity for the second peak is $L = 2.4 \times 10^{40}$ erg s^{-1} and the total energy release during the outburst is $L > 4.1 \times 10^{47}$ erg. This is only a lower limit, as the first outburst is not covered well enough to put a tight constraint on the energy.
7. During peak, the spectrum shows a cold photospheric continuum, combined with low expansion velocities (∼300 km s^{-1}) for Hα, Fe II, and low-energy ionization elements, which display a P-Cygni profile.
8. The light curve after the second outburst is defined by a short decline phase (∼40 days), a "plateau" phase (∼60 days) in *riz* bands and a second decline phase. The photospheric radius at the beginning of each phase was ∼ 6500 $R_\odot$, 4300 $R_\odot$, and 5800 $R_\odot$, respectively.
9. The Hα line shows initially a blueshifted absorption component at −500 km s^{-1}, which develops into an emission profile at epochs +30 days or later.
10. The spectrum shows the formation of molecular bands after 100 days of the outburst, which suggests the fast formation of dust in the system.
11. The best fit for the progenitor is an F-type giant with a luminosity of $L \sim 8.7 \times 10^4$ $L_\odot$ and initial mass of 18 ± 1. The estimated age of the star is ∼10 Myr, which places it in the Hertzsprung–Russell gap. This estimate is qualitatively consistent with the young stellar population surrounding the progenitor, although high-accuracy photometry will be needed to provide a quantitative answer.
12. In the binary case scenario, assuming that the primary is overfilling its RL, the binary system is initially on a wide orbit, with periods between 600 and 270 days (for $q = 1$, and $q = 18$ respectively). By the end of the common envelope phase, the fate of the system depends on the model. While the simple energy formalism anticipates the complete merger of the system, binary evolution models favor the survival of the binary stellar component with a 260−290 day period.

Although the nature of the object is yet not entirely clear, its resemblance to other transients from the same LRN family points toward a possible binary origin. The unusual location of the progenitor star in the Hertzsprung gap supports the

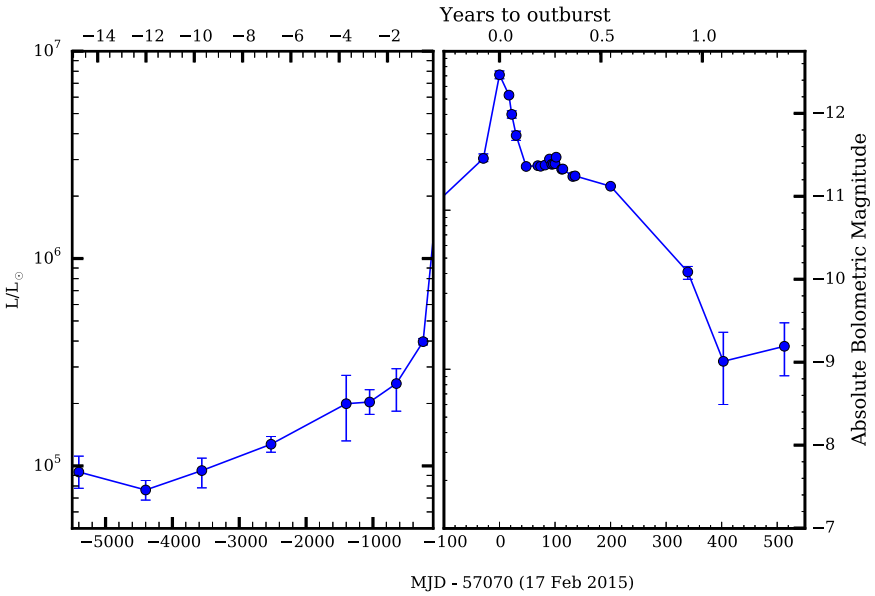

Figure 8. The evolution of the blackbody luminosity of M101-OT. The first peak is not present, as there were not enough photometric measurements for a reliable fit. The measurements for epochs after +200 days were derived using NIR bands only.

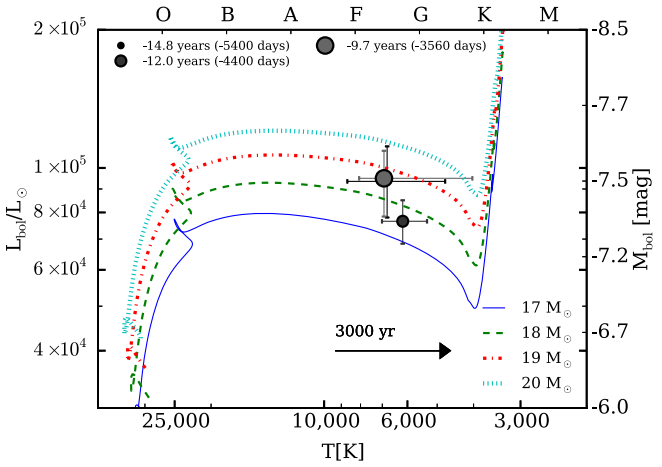

Figure 9. The position of the progenitor of M101-OT for the first three initial epochs older than 2500 days, when L_{bol} is constant. The size of the point encodes the epoch of the observation relative to discovery. Stellar evolutionary tracks for single-star models (Eldridge & Tout 2004) are shown for stars with initial masses from 17–20 $M_\odot$. To provide a graphic example of the short life of stars in the progenitor region, the arrow shows the temperature locus covered by an 18 $M_\odot$ star in only 3000 years.

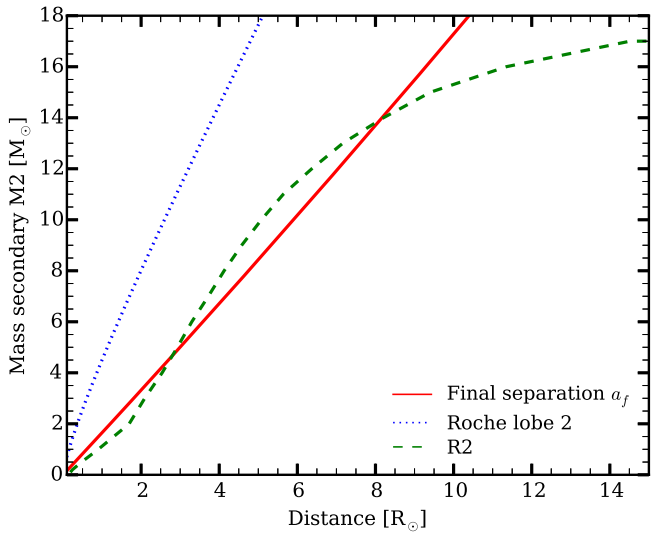

Figure 10. Final state of the binary system assuming that all the envelope is ejected at the expense of the orbital energy, reducing the separation of the components from a_i to a_f. The primary star has an initial mass of 18 $M_\odot$ and an envelope of 13 $M_\odot$. The initial separation has been estimated from the radius of the primary (see text). The red solid line indicates the boundary final separation, a_f, when the release of orbital energy equals the binding energy of the envelope for a given secondary mass $M2$. The blue dotted line shows the RL of the secondary star for the given a_f, secondary mass $M2$, and the core of the remnant $M1_c = 5$ $M_\odot$. The dashed green line shows the radius of the secondary star at 9.9 Myr.

hypothesis that the most massive component had expanded beyond its RL, initiating the CE phase. The outbursts detected for M101-OT suggest that this CE was ejected on dynamical timescales, leaving either a surviving close binary pair or a new merged object.

We have discussed the past and present evolution of this unusual transient in M101; discussion of its future and the fate of its remnant will have to await further observations in the IR bands.

The research leading to these results has received funding from the European Union Seventh Framework Programme ([FP7/2007-2013] under grant agreement no. 264895. This work was partly supported by the European Union FP7 programme through ERC grant no. 320360. This work was supported, in whole or in part, by the European Science Foundation under the GREAT ESF RNP programme. This work was supported by the GROWTH project funded by the National Science Foundation under grant no. 1545949. LANL participation in iPTF was funded by the US Department of Energy as part of the Laboratory Directed Research and Development program. Part of this research was carried out at the Jet Propulsion Laboratory, California Institute of Technology, under a contract with the National Aeronautics and Space Administration. Based on observations obtained with MegaPrime/MegaCam, a joint project of CFHT and CEA/IRFU, at the Canada–France–Hawaii Telescope (CFHT), which is

operated by the National Research Council (NRC) of Canada, the Institut National des Science de l'Univers of the Centre National de la Recherche Scientifique (CNRS) of France, and the University of Hawaii. This work is based in part on data products produced at Terapix available at the Canadian Astronomy Data Centre as part of the Canada–France–Hawaii Telescope Legacy Survey, a collaborative project of NRC and CNRS. This paper makes use of data obtained from the Isaac Newton Group Archive, which is maintained as part of the CASU Astronomical Data Centre at the Institute of Astronomy, Cambridge. This work is partly based on observations obtained with the Nordic Optical Telescope, operated by the Nordic Optical Telescope Scientific Association at the Observatorio del Roque de los Muchachos, La Palma, Spain. This work is partly based on observations made with the William Herschell Telescope operated on the island of La Palma by the Isaac Newton Group in the Spanish Observatorio del Roque de los Muchachos of the Instituto de Astrofsica de Canarias. The Gran Telescopio Canarias (GTC) operated on the island of La Palma at the Spanish Observatorio del Roque de los Muchachos of the Instituto de Astrofisica de Canarias. This work is partly based on data from Copernico 1.82 m telescope operated by INAF Osservatorio Astronomico di Padova. NER, AP, GT, and MT are partially supported by the PRIN-INAF 2014 with the project "Transient universe: unveiling new types of stellar explosions with PESSTO." Finally, NBM would like to thank the anonymous referee, who helped to improve the manuscript, Robert G. Izzard, Philipp Podsiadlowski, Lars Bildsten, E. Sterl Phinney, and Noam Soker for helpful discussions, and Pablo and Lucia Solis, and Israel Zenteno for the motivation.

Facilities: Asiago:Copernico, CFHT, GTC, Hale, ING: Newton, ING:Herschel, Keck:I, LBT, Liverpool:2m, NOT, PO:1.2m, PO:1.5m, PS1, Sloan, Spitzer, UKIRT.

Software: BPASS v1.0, BPASS v2.0, EMCEE (Foreman-Mackey et al. 2013), IRAF, NOTCAM (v2.54), PTFIDE (Masci et al. 2016), PYRAF, SNOoPY.

APPENDIX
PHOTOMETRY TABLES

REFERENCES

Adams, S. M., Kochanek, C. S., Prieto, J. L., et al. 2016, MNRAS, 460, 1645
Ahn, C. P., Alexandroff, R., Allende Prieto, C., et al. 2014, ApJS, 211, 17
Andrews, J. E., Krafton, K. M., Clayton, G. C., et al. 2016, MNRAS, 457, 3241
Bagnulo, S., Jehin, E., Ledoux, C., et al. 2003, Msngr, 114, 10
Bevan, A., & Barlow, M. J. 2016, MNRAS, 456, 1269
Bond, H. E., Bedin, L. R., Bonanos, A. Z., et al. 2009, ApJL, 695, L154
Bond, H. E., Henden, A., Levay, Z. G., et al. 2003, Natur, 422, 405
Botticella, M. T., Pastorello, A., Smartt, S. J., et al. 2009, MNRAS, 398, 1041
Cao, Y., Kasliwal, M. M., Chen, G., & Arcavi, I. 2015, ATel, 7070, 1
Cenko, S. B., Fox, D. B., Moon, D.-S., et al. 2006, PASP, 118, 1396
de Kool, M. 1990, ApJ, 358, 189
de Vaucouleurs, G., de Vaucouleurs, A., Corwin, H. G., Jr., et al. 1991, S&T, 82, 621
Eggleton, P. P. 1983, ApJ, 268, 368
Eldridge, J. J., & Tout, C. A. 2004, MNRAS, 353, 87
Fazio, G. G., Hora, J. L., Allen, L. E., et al. 2004, ApJS, 154, 10
Foley, R. J., Berger, E., Fox, O., et al. 2011, ApJ, 732, 32
Foreman-Mackey, D., Hogg, D. W., Lang, D., & Goodman, J. 2013, PASP, 125, 306
Fraser, M., Inserra, C., Jerkstrand, A., et al. 2013, MNRAS, 433, 1312
Gerke, J., Adams, S. M., Kochanek, C. S., & Stanek, K. Z. 2015, ATel, 7069, 1
Goranskij, V. P., Barsukova, E. A., Spiridonova, O. I., et al. 2016, AstBu, 71, 82
Goranskij, V. P., Cherjasov, D. V., Safonov, B. S., et al. 2015, ATel, 7206, 1
Gröningsson, P., Fransson, C., Lundqvist, P., et al. 2008, A&A, 479, 761
Gwyn, S. D. J. 2008, PASP, 120, 212
Humphreys, R. M., & Davidson, K. 1994, PASP, 106, 1025
Iben, I., Jr., & Tutukov, A. V. 1992, ApJ, 389, 369
Ivanova, N., Justham, S., Avendano Nandez, J. L., & Lombardi, J. C. 2013a, Sci, 339, 433
Ivanova, N., Justham, S., Chen, X., et al. 2013b, A&Ar, 21, 59
Kamiński, T., Schmidt, M., & Tylenda, R. 2010, A&A, 522, A75
Kankare, E., Ergon, M., Bufano, F., et al. 2012, MNRAS, 424, 855
Kankare, E., Kotak, R., Pastorello, A., et al. 2015, A&A, 581, L4
Kashi, A., Frankowski, A., & Soker, N. 2010, ApJL, 709, L11
Kasliwal, M. M. 2011, BASI, 39, 375
Kasliwal, M. M., Kulkarni, S. R., Arcavi, I., et al. 2011, ApJ, 730, 134
Kelly, P., Van Dyk, S., Fox, O., Filippenko, A. V., & Foley, R. 2015, ATel, 7082, 1
Khan, R., Stanek, K. Z., Prieto, J. L., et al. 2010, ApJ, 715, 1094
Kochanek, C. S. 2011, ApJ, 741, 37
Kochanek, C. S., Adams, S. M., & Belczynski, K. 2014, MNRAS, 443, 1319
Kulkarni, S. R., Ofek, E. O., Rau, A., et al. 2007, Natur, 447, 458
Kurtenkov, A. A., Pessev, P., Tomov, T., et al. 2015, A&A, 578, L10
Liermann, A., Schnurr, O., Kraus, M., et al. 2014, MNRAS, 443, 947
MacLeod, M., Macias, P., Ramirez-Ruiz, E., et al. 2016, arXiv:1605.01493
Magnier, E. A., Schlafly, E., Finkbeiner, D., et al. 2013, ApJS, 205, 20
Martini, P., Wagner, R. M., Tomaney, A., et al. 1999, AJ, 118, 1034
Masci, F., Laher, R., Rebbapragada, U., et al. 2016, arXiv:1608.01733
Mason, E., Diaz, M., Williams, R. E., Preston, G., & Bensby, T. 2010, A&A, 516, A108
Mauerhan, J. C., Smith, N., Filippenko, A. V., et al. 2013, MNRAS, 430, 1801
Mauerhan, J. C., Van Dyk, S. D., Graham, M. L., et al. 2015, MNRAS, 447, 1922
Nandez, J. L. A., Ivanova, N., & Lombardi, J. C., Jr. 2014, ApJ, 786, 39
Nugent, P. E., Sullivan, M., Cenko, S. B., et al. 2011, Natur, 480, 344
Ofek, E. O., Kulkarni, S. R., Rau, A., et al. 2008, ApJ, 674, 447
Ofek, E. O., Laher, R., Law, N., et al. 2012, PASP, 124, 62
Paczynski, B. 1976, in IAU Symp. 73, Structure and Evolution of Close Binary Systems, ed. P. Eggleton, S. Milton, & J. Whelan (Dordrecht: Reidel), 75
Pastorello, A., Cappellaro, E., Inserra, C., et al. 2013, ApJ, 767, 1
Pastorello, A., Della Valle, M., Smartt, S. J., et al. 2007, Natur, 449, 1
Pejcha, O., Metzger, B. D., & Tomida, K. 2016, MNRAS, 455, 4351
Perryman, M. A. C., de Boer, K. S., Gilmore, G., et al. 2001, A&A, 369, 339
Prieto, J. L., Kistler, M. D., Thompson, T. A., et al. 2008, ApJL, 681, L9
Prieto, J. L., Sellgren, K., Thompson, T. A., & Kochanek, C. S. 2009, ApJ, 705, 1425
Rau, A., Ofek, E. O., Kulkarni, S. R., et al. 2008, ApJ, 682, 1205
Retter, A., & Marom, A. 2003, MNRAS, 345, L25
Rich, R. M., Mould, J., Picard, A., Frogel, J. A., & Davies, R. 1989, ApJL, 341, L51
Rushton, M. T., Geballe, T. R., Filippenko, A. V., et al. 2005, MNRAS, 360, 1281
Schlafly, E. F., & Finkbeiner, D. P. 2011, ApJ, 737, 103
Schlafly, E. F., Finkbeiner, D. P., Jurić, M., et al. 2012, ApJ, 756, 158
Shappee, B. J., & Stanek, K. Z. 2011, ApJ, 733, 124
Smith, N. 2004, MNRAS, 349, L31
Smith, N., Andrews, J. E., Mauerhan, J. C., et al. 2016a, MNRAS, 455, 3546
Smith, N., Andrews, J. E., Van Dyk, S. D., et al. 2016b, MNRAS, 458, 950
Smith, N., Li, W., Silverman, J. M., Ganeshalingam, M., & Filippenko, A. V. 2011, MNRAS, 415, 773
Smith, N., Mauerhan, J. C., Cenko, S. B., et al. 2015, MNRAS, 449, 1876
Smith, N., Miller, A., Li, W., et al. 2010, AJ, 139, 1451
Smith, N., Vink, J. S., & de Koter, A. 2004, ApJ, 615, 475
Soker, N. 2016, NewA, 47, 16
Soker, N., & Kashi, A. 2016, arXiv:1605.07382
Soker, N., & Tylenda, R. 2003, ApJL, 582, L105
Sparks, W. B., Bond, H. E., Cracraft, M., et al. 2008, AJ, 135, 605
Stanway, E. R., Eldridge, J. J., & Becker, G. D. 2016, MNRAS, 456, 485
Thompson, T. A., Prieto, J. L., Stanek, K. Z., et al. 2009, ApJ, 705, 1364
Tonry, J. L., Stubbs, C. W., Lykke, K. R., et al. 2012, ApJ, 750, 99
Tylenda, R., Hajduk, M., Kamiński, T., et al. 2011, A&A, 528, A114
Tylenda, R., Kamiński, T., Udalski, A., et al. 2013, A&A, 555, A16
Walborn, N. R., Stahl, O., Gamen, R. C., et al. 2008, ApJL, 683, L33
Williams, S. C., Darnley, M. J., Bode, M. F., & Steele, I. A. 2015, ApJL, 805, L18
Wolf, B. 1989, in IAU Coll. 113: Physics of Luminous Blue Variables, ed. K. Davidson, A. F. J. Moffat, & H. J. G. L. M. Lamers (Dordrecht: Kluwer), 91
Yaron, O., & Gal-Yam, A. 2012, PASP, 124, 668